Modal reduction of a parametrically forced confined viscous flow

Jason Yalim,[*] Bruno D. Welfert,[†] and Juan M. Lopez[‡]
School of Mathematical and Statistical Sciences, Arizona State University, Tempe, Arizona 85287, USA

(Received 15 January 2019; published 14 October 2019)

An exact reduction of parametrically and periodically forced linear dynamical systems to modal dynamics in low-dimensional subspaces is possible when the operators involved commute with one another. We describe how a modal analysis may still be possible in the noncommuting case. The approach is illustrated with the determination of neutral curves for a stably and linearly stratified fluid in a square cavity under harmonically modulated gravitational forcing. In this example, the noncommutation of operators in the resulting Mathieu system is a direct consequence of the combined action of diffusion and wall confinement effects. An ansatz for modal diffusion is proposed, which enables remarkably predictive estimates of neutral curves via superposition of modal responses.

DOI: 10.1103/PhysRevFluids.4.103903

I. INTRODUCTION

The dynamics of physical phenomena are often described via Newton's second law. Restoring forces, such as Coriolis effects in rotating flows or buoyancy forces in stratified flows, lead to models that are analogous to coupled spring-mass systems. In the absence of friction and/or spatial confinement, external periodic forcing results in dynamics that can be expressed as a superposition of the modal responses of decoupled oscillators. In the context of surface waves of a homogeneous fluid in a large container subjected to vertical oscillations of angular frequency Ω, Benjamin and Ursell [1] were the first to make this observation. Their analysis, made under the assumption of vanishing viscosity, led to a Mathieu partial differential equation (PDE) for the free surface elevation. This PDE was reduced to scalar modal Mathieu equations, which satisfactorily reproduced experimental results; small discrepancies were attributed to meniscus and viscous boundary layer effects at the bottom wall of the container. Viscosity dampens the surface oscillations, which can nevertheless be sustained via the parametric forcing if the forcing amplitude is sufficiently large. Internal gravity waves in a fully confined and continuously stably stratified fluid were later studied with similar outcomes [2,3].

Subsequent studies involving parametric forcing of Faraday waves [4–6], internal gravity waves [7], and Rayleigh-Bénard convection [8] with viscous fluids in finite-sized containers subjected to harmonic vertical oscillations showed that in order to sustain the waves, larger forcing amplitudes are required to overcome the strong viscous dissipation in the boundary layers of the container walls. These viscous effects are notoriously difficult to quantify. The typical ansatz $-\nu|\boldsymbol{k}|^2$ for the action of $\nu\nabla^2$ representing viscous diffusion, where ν is the kinematic viscosity and $|\boldsymbol{k}|$ is the Euclidean magnitude of the wave vector $\boldsymbol{k}$, relies on the existence of a wavelike response that is typically associated with responses in unbounded domains or ideal (inviscid) fluids, and grossly underestimates the viscous contributions in boundary layers. As noted in Ref. [9], even

[*]yalim@asu.edu
[†]Corresponding author: welfert@asu.edu
[‡]jmlopez@asu.edu

small viscosity can also nontrivially modify the interior flow away from boundary layers. Various corrections based on powers of $\sqrt{\nu|\boldsymbol{k}|^2/\Omega}$ have been proposed to improve comparisons between model and experimental results [10–12], but those usually assume small ν, $|\boldsymbol{k}|$, and/or large Ω, and introduce nonlocalization not only in space but also in time due to the fractional powers of $|\boldsymbol{k}|^2$ and Ω, at least for low to moderate viscosity [13,14]. The global nature of these corrections is ultimately rooted in the noncommutativity of the differential operators involved in the damped Mathieu PDE as a result of viscosity and confinement. The lack of operator commutativity prevents a standard modal analysis via simultaneous diagonalization of the operators and a simple superposition of scalar Mathieu responses.

We show how responses to scalar damped Mathieu equations can in fact be superposed in confined configurations of viscous fluids under parametric excitation, and we obtain a reliable predictive estimate of the instability curves over a wide range of forcing frequency, provided an appropriate ansatz for diffusive effects is used. The proposed strategy relies on a simple ad hoc model of modal diffusion based on data of critical forcing amplitudes at selected forcing frequencies and viscosities, which are obtained from a numerical Floquet analysis of the full problem. Such a strategy provides an economical alternative to a global Floquet analysis of the parametrically forced Navier-Stokes-Boussinesq equations.

Our approach is illustrated with a study of the onset of instability of a linearly stratified fluid in a square cavity subjected to harmonically modulated gravitational acceleration. It is closely related to the physical experiments of Benielli and Sommeria [7], the Floquet analysis of the full problem in Yalim *et al.* [15], and the numerical exploration conducted beyond criticality in Ref. [16]. The analogy made in Ref. [7] between the stratified fluid's response to the vertical oscillations and that of a parametrically excited pendulum modeled by a Mathieu equation is hampered by the modal expression used for boundary dissipation [Ref. [7], Eq. (5.5)] vanishing for horizontal wave vectors and neglecting viscous effects at lateral walls, whose only role in their model is to quantize these wave vectors. The discrepancies between theory and experiments were correctly attributed to unaccounted friction due to boundary layer effects. Our results show that a proper evaluation of these effects via an ad hoc modal dissipation model can restore the agreement over a broad range of parameters.

II. MODEL FORMULATION

The model problem consists of a square cavity of side lengths L that is completely filled with a fluid of kinematic viscosity ν, thermal diffusivity κ, and coefficient of volume expansion β. The velocity boundary conditions are no-slip on all walls. The cavity sidewalls are thermally insulated (adiabatic) while the endwalls are held at constant temperatures, T_T on the top wall and T_B on the bottom wall. The nondimensional temperature is $T = (T^* - T_\mathrm{B})/\Delta T - 0.5$, where T^* is the dimensional temperature and $\Delta T = T_\mathrm{T} - T_\mathrm{B} > 0$. Gravity g acts downward. In the absence of any other external force, the fluid is linearly stratified. The cavity is subjected to harmonic oscillations in the vertical direction with angular frequency Ω and amplitude ℓ.

The system is nondimensionalized using length scale L and time scale $1/N$, where $N = \sqrt{g\beta\Delta T/L}$ is the buoyancy frequency. In a frame of reference attached to the oscillating cavity, the nondimensional governing equations using the Boussinesq approximation are

$$\partial_t \boldsymbol{u} + \boldsymbol{u}\cdot\boldsymbol{\nabla}\boldsymbol{u} = -\boldsymbol{\nabla}p + \frac{1}{R_\mathrm{N}}\nabla^2\boldsymbol{u} + f(t)T\boldsymbol{e}_z, \quad \boldsymbol{\nabla}\cdot\boldsymbol{u} = \boldsymbol{0}, \quad \partial_t T + \boldsymbol{u}\cdot\boldsymbol{\nabla}T = \frac{1}{\sigma R_\mathrm{N}}\nabla^2 T, \tag{1}$$

where p is the reduced pressure, $\boldsymbol{e}_z$ is the unit vector in the vertical direction, and

$$f(t) = 1 + \alpha\cos(\omega t) \tag{2}$$

is the resulting modulated (gravity) body force. The horizontal and vertical components of the velocity in $x \in [-0.5, 0.5]$ and $z \in [-0.5, 0.5]$ directions are u and w. A schematic of the nondimensionalized configuration is shown in Fig. 1.

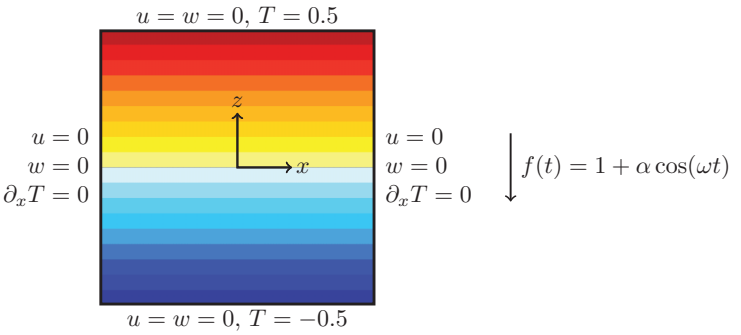

FIG. 1. Schematic showing the basic state isotherms, boundary conditions, coordinate system, and body forcing.

The system is governed by four nondimensional parameters:

$$\begin{array}{ll} \text{Buoyancy number,} & R_{\mathrm{N}} = NL^2/\nu; \\ \text{Prandtl number,} & \sigma = \nu/\kappa; \\ \text{forcing frequency,} & \omega = \Omega/N; \\ \text{forcing amplitude,} & \alpha = \Omega^2\ell/g. \end{array} \tag{3}$$

The restriction $0 < \alpha \leqslant 1$ guarantees that the vertical acceleration of the cavity points in the downward direction at all times, and the linearly stratified fluid remains convectively stable. Under this assumption, it will be sufficient to consider $0 < \omega \leqslant 2.5$.

The static and stably stratified base state, $u_b = 0$, $w_b = 0$, and $T = z$, is an equilibrium solution for any σ, ω, α, and $R_{\mathrm{N}} \geqslant 0$. The time evolution of small perturbations $(u, w, \theta) = (u - u_b, w - w_b, T - z)$ about this static equilibrium is governed by the nondimensionalized Navier-Stokes-Boussinesq equations (1) linearized about the base state,

$$\begin{aligned} \partial_t u &= -\partial_x p + \frac{1}{R_{\mathrm{N}}}\nabla^2 u, \\ \partial_t w &= -\partial_z p + \frac{1}{R_{\mathrm{N}}}\nabla^2 w + f(t)\theta, \\ \partial_t \theta &= -w + \frac{1}{\sigma R_{\mathrm{N}}}\nabla^2\theta, \\ \partial_x u + \partial_z w &= 0. \end{aligned} \tag{4}$$

The incompressibility condition yields a Poisson equation for the pressure p,

$$\nabla^2 p = f(t)\partial_z\theta, \tag{5}$$

so that

$$\mathcal{L}\theta = -\frac{1}{f(t)}\partial_z p + \theta \tag{6}$$

defines a bounded linear operator $\mathcal{L}$ that satisfies

$$\nabla^2\mathcal{L}\theta = -\frac{1}{f(t)}\partial_z\nabla^2 p + \nabla^2\theta = -\partial_z^2\theta + \nabla^2\theta = \partial_x^2\theta. \tag{7}$$

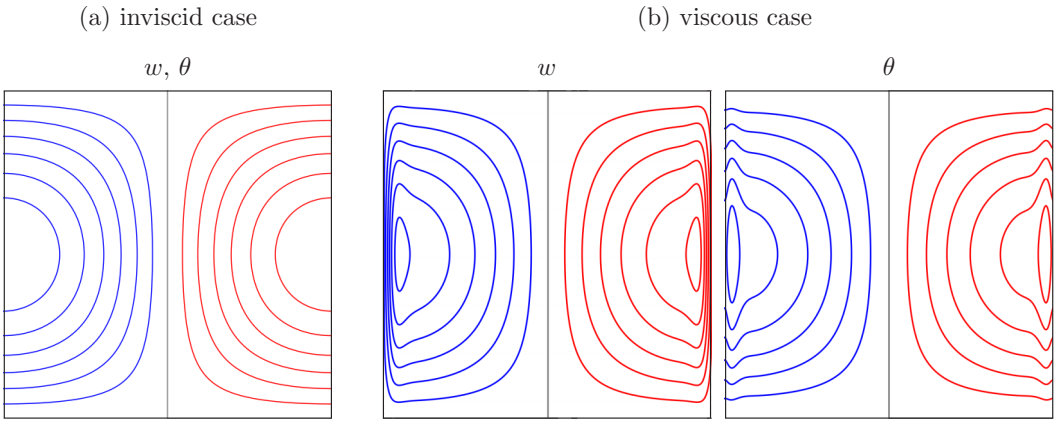

FIG. 2. Contour levels with red positive and blue negative for the perturbation vertical velocity w and perturbation temperature θ obtained at $\omega \approx \sqrt{2}$ for (a) the inviscid and unforced $a_{1:1}$ ($R_N \to \infty$), and (b) the viscous w and θ at $R_N = 2 \times 10^4$ and $\sigma = 1$ for α near onset obtained from Floquet analysis. The magnitude of eigenmodes (w, θ) is arbitrary, but that of θ relative to w is not.

The time evolution of w and θ can then be written as

$$\partial_t \begin{bmatrix} w \\ \theta \end{bmatrix} = \mathcal{A}(t) \begin{bmatrix} w \\ \theta \end{bmatrix}, \quad \mathcal{A}(t) = \begin{bmatrix} \frac{1}{R_N}\nabla^2 & f(t)\mathcal{L} \\ -\mathcal{I} & \frac{1}{\sigma R_N}\nabla^2 \end{bmatrix}, \tag{8}$$

where $\mathcal{I}$ is the identity operator.

III. STABILITY OF THE PARAMETRICALLY FORCED BASE STATE

A. Inviscid case

The stability of (8) depends on the spectrum of the monodromy operator. In the inviscid limit $R_N \to \infty$, the Laplacian terms vanish. Diagonalization of $\mathcal{L}$ reduces the problem of studying the monodromy operator of (8) to the study of the system of 2×2 monodromy matrices

$$\frac{d}{dt} \begin{bmatrix} w_k \\ \theta_k \end{bmatrix} = A_k(t) \begin{bmatrix} w_k \\ \theta_k \end{bmatrix}, \quad A_k(t) = \begin{bmatrix} 0 & f(t)\lambda_k \\ -1 & 0 \end{bmatrix}, \tag{9}$$

describing the time evolution of solutions of (8):

$$\begin{bmatrix} w \\ \theta \end{bmatrix} = \begin{bmatrix} w_k(t) \\ \theta_k(t) \end{bmatrix} a_k(x, z), \tag{10}$$

where the index $\boldsymbol{k} = (m\pi, n\pi) = m{:}n$, with positive integers m and n. Here, $a_k(x, z) = \cos m\pi(x + 0.5) \sin n\pi(z + 0.5)$ are the eigenmodes of $\mathcal{L}$, and they are solutions of the generalized eigenvalue problems

$$\lambda_k \nabla^2 a_k = \partial_x^2 a_k, \tag{11}$$

with boundary conditions $a_k(x, \pm 0.5) = \partial_x a_k(\pm 0.5, z) = 0$. The corresponding eigenvalues are [3]

$$\lambda_k = \frac{m^2}{m^2 + n^2}. \tag{12}$$

Note that the perturbation vertical velocity w obtained from (10) only vanishes on the top and bottom boundaries, which is consistent with the impermeability condition imposed at boundaries in the inviscid case. Figure 2(a) shows the spatial structure of the inviscid mode $a_{1:1}$, describing both w and θ. In this inviscid setting, w and θ have the same spatial structure.

Eliminating $w_{\boldsymbol{k}}$ in Eq. (9) leads to the Mathieu equation

$$\theta_{\boldsymbol{k}}'' + f(t)\lambda_{\boldsymbol{k}}\theta_{\boldsymbol{k}} = 0. \tag{13}$$

This equation has a rich history, dating back to Mathieu's work on Poisson equations in elliptic domains [17]. It has found numerous applications [18,19], and its theory is well-established [20,21]. In particular, the eigenvalues of the monodromy matrix of (9) with modulus 1 can only be ± 1, occurring at the edge of an infinite sequence of horns emanating from frequencies $\omega = 2\lambda_{\boldsymbol{k}}^{1/2}/\ell$, with $\ell = 1, 2, \ldots$, at forcing amplitude $\alpha = 0$ in the stability diagram delineating stable regions in (ω, α)-space with either subharmonic (ℓ odd) or synchronous (ℓ even) periodic solutions. The stability diagram is often referred to as the Ince-Strutt, Strutt, or Strutt-Ince diagram [21].

B. Viscous case

In the viscous case ($R_{\mathrm{N}} < \infty$), a standard stability estimate using the L_2 norm shows that the global perturbation L_2 energy, $\|u\|^2 + \|w\|^2 + \|\theta\|^2$, decreases for $\alpha > 0$ small enough. The onset of instability coincides with the characteristic multipliers crossing the unit circle in the complex plane, which has been observed numerically to occur only through ± 1 in this problem. The first occurrence of a multiplier exiting the unit disk at -1 (subharmonic response) or $+1$ (synchronous response) determines two critical curves in (ω, α) space, illustrated in Ref. [15] for $R_{\mathrm{N}} = 2 \times 10^4$ and $\sigma = 1$, and reproduced here in Figs. 3 and 4.

At $\omega = 1.41 \approx \sqrt{2}$, the instability occurs at $\alpha \approx 0.07$ via a flip bifurcation (subharmonic response). Contours of the perturbation vertical velocity w and the perturbation temperature θ of the corresponding eigenmode of the monodromy operator are shown in Fig. 2(b) and illustrate how viscosity affects the response (w, θ) at the onset of instability, compared to the inviscid case. The forced viscous modes w and θ both broadly resemble the inviscid mode $a_{1:1}$, except that the viscous velocity satisfies the no-slip condition $w = 0$ on the side boundaries. The difference in boundary conditions for w on the sidewalls ($\partial_x w = \partial_{xt}\theta = 0$ in the inviscid case and $w = 0$ in the viscous case) introduces distortions due to the formation of boundary layers—these boundary layers in w also distort the perturbation temperature distribution in the boundary layer regions, even though the boundary condition on θ is the same in both the viscous and inviscid setting, i.e., the sidewalls are insulating with $\theta_x = 0$. These effects lead to the loss of commutativity of the operators ∇^2 and $\mathcal{L}$. This prevents an exact modal reduction of (8) to a superposition of first-order Mathieu equations (9).

An approximating modal reduction is nevertheless desirable, as it delivers considerable savings in the computational cost of evaluating critical curves over a large range of forcing frequencies, especially when compared to the computation of the monodromy matrix in the Floquet analysis. A widely used approach is to continue replacing, as in the inviscid case, the action of $\mathcal{A}(t)$ on the Floquet eigenmodes by its action on the inviscid modes (10). This ansatz leads to a system of the form (9) again, but with

$$\frac{d}{dt}\begin{bmatrix} w_{\boldsymbol{k}} \\ \theta_{\boldsymbol{k}} \end{bmatrix} = A_{\boldsymbol{k}}(t)\begin{bmatrix} w_{\boldsymbol{k}} \\ \theta_{\boldsymbol{k}} \end{bmatrix}, \quad A_{\boldsymbol{k}}(t) = \begin{bmatrix} \frac{1}{R_{\mathrm{N}}}\delta_{\boldsymbol{k}} & f(t)\lambda_{\boldsymbol{k}} \\ -1 & \frac{1}{\sigma R_{\mathrm{N}}}\delta_{\boldsymbol{k}} \end{bmatrix}, \tag{14}$$

where

$$\delta_{\boldsymbol{k}} = -\pi^2(m^2 + n^2). \tag{15}$$

Elimination of $w_{\boldsymbol{k}}$ in Eq. (14) yields the second-order equation

$$\theta_{\boldsymbol{k}}'' + c_{\boldsymbol{k}}\theta_{\boldsymbol{k}}' + g_{\boldsymbol{k}}(t)\,\theta_{\boldsymbol{k}} = 0, \tag{16}$$

where $c_{\boldsymbol{k}} = -\mathrm{trace}[A_{\boldsymbol{k}}(t)]$ and $g_{\boldsymbol{k}}(t) = \det[A_{\boldsymbol{k}}(t)]$. The stability diagram of this damped Mathieu equation consists of tongues in (ω, α) space with boundaries alternately corresponding to

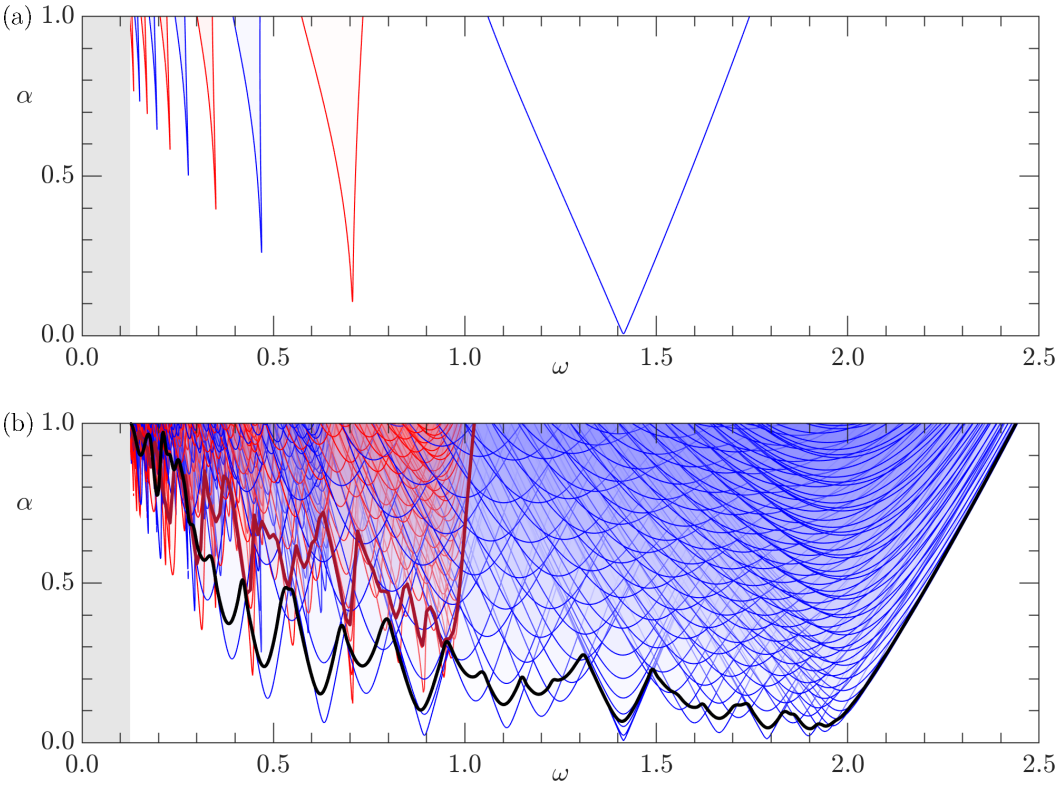

FIG. 3. (a) Instability tongues of the Mathieu system associated with the m:$n = 1$:1 mode at $R_N = 2 \times 10^4$ and $\sigma = 1$ in (ω, α) parameter space. (b) Superposition of viscous Mathieu stability tongues (thin blue curves for subharmonic and thin red curves for synchronous responses) at $R_N = 2 \times 10^4$ and $\sigma = 1$ associated with modes m:n for $m, n \geqslant 1$. The subharmonic (thick black) and synchronous (thick red) stability boundaries determined from the Floquet analysis of the Navier-Stokes-Boussinesq system are also shown. The tongues accumulating at low frequencies are narrower and more difficult to estimate (gray area).

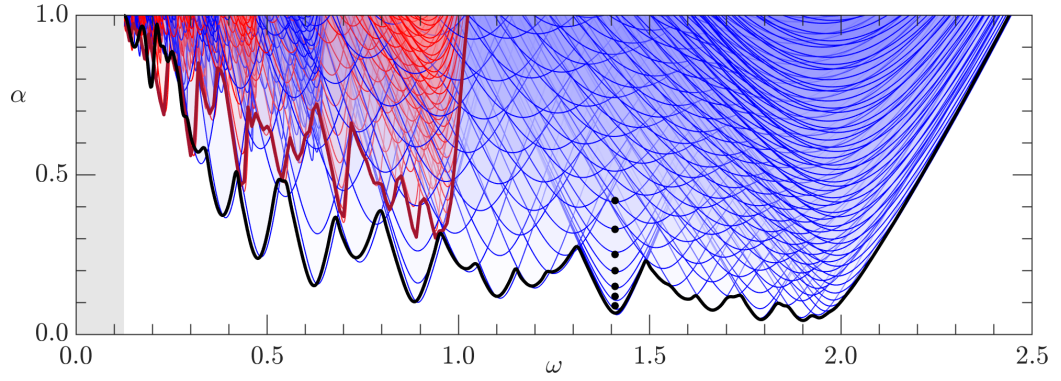

FIG. 4. Same as in Fig. 3(b), but now using the corrected diagonal coefficients (21) in Eq. (14) with $\gamma = 20$. The black dots correspond to critical Floquet results for the viscous m:m modes with $1 \leqslant m \leqslant 8$.

TABLE I. μ_ℓ versus ℓ for mode 1:1.

ℓ	1	2	3	4	5	6	7	8	9	10
μ_ℓ	2.00	2.00	1.84	1.72	1.63	1.55	1.49	1.45	1.41	1.38

subharmonic and synchronous periodic solutions [22], shown in Fig. 3(a) for the mode $m{:}n = 1{:}1$ at $R_N = 2 \times 10^4$ and $\sigma = 1$. These tongues are efficiently determined, as an alternative to Floquet analysis or other asymptotic methods typically used with small α, as the zero contour level of a Hill continued fraction, which results from applying harmonic balance to Mathieu's equation [21]; see Appendix A. Each tongue corresponds to a mode of instability of the linearly stratified base state with the same 1:1 spatial response to different forcing frequencies $\omega_\ell \approx 2\lambda_{1:1}^{1/2}/\ell = \sqrt{2}/\ell$, slightly detuned from the inviscid values, with a minimum forcing amplitude $\alpha_\ell \approx \mu_\ell Q_{1:1}^{1/\ell}$, where $Q_{1:1} = c_{1:1}/\lambda_{1:1}^{1/2}$ measures the dissipation for mode 1:1. The constants μ_ℓ, $\ell = 1, \ldots, 10$, estimated from the minimum critical amplitudes α_ℓ of the first ten tongues [visible in Fig. 3(a)] and $Q_{1:1} \approx 2.8 \times 10^{-3}$ for mode 1:1 at $R_N = 2 \times 10^4$ and $\sigma = 1$, are listed in Table I. The value $\mu_1 = 2.00$ relating the minimal critical amplitude α to the friction coefficient c at the principal 1:1 tongue is well-known; for example, see Ref. [22], p. 1256. Figure 3(a) clearly illustrates that the same spatial mode can be excited at many different forcing frequencies ω, however they require different forcing amplitudes α to overcome viscous damping at those different frequencies. This is due to the oscillatory boundary layers on the walls having structures and intensities that depend on both R_N and ω, and these have nonlocal effects, an issue that is well recognized [9].

The superposition of the resulting curves for all wave numbers $\boldsymbol{k}$ is shown in Fig. 3(b), together with the subharmonic (thick blue) and synchronous (thick red) critical curves computed via Floquet analysis in Ref. [15]. To the best of our knowledge, this figure is the first instance of a frequency-wide model of actual stability boundaries of a base state in an Ince-Strutt diagram. Not surprisingly, the ansatz (14), based on the action of spatial operators on inviscid modes, tends to underestimate viscous effects in boundary layers, lowering the critical amplitude α for onset of instability across the whole ω spectrum as a result. This is more so at $\omega \leqslant \sqrt{2}$, for which the wave vectors $\boldsymbol{k}$ are predominantly vertical ($m \leqslant n$) and are more affected by the strong boundary layers on the sidewalls.

C. Confined viscous case

To take the additional diffusion occurring in boundary layers into account, the modal action of ∇^2 is estimated via Rayleigh quotients

$$\mathcal{R}(\nabla^2, w) = \frac{(\nabla^2 w, w)}{(w, w)} = -\frac{\|\nabla w\|^2}{\|w\|^2} \quad \text{and} \quad \mathcal{R}(\nabla^2, \theta) = \frac{(\nabla^2 \theta, \theta)}{(\theta, \theta)} = -\frac{\|\nabla \theta\|^2}{\|\theta\|^2}, \tag{17}$$

evaluated on selected viscous Floquet eigenmodes $w_{\boldsymbol{k}}$ and $\theta_{\boldsymbol{k}}$, where $(\cdot, \cdot)$ is the L_2 inner product. Here the modes $\boldsymbol{k} = m{:}m$ with $1 \leqslant m \leqslant 8$ are selected and evaluated at or close to the tip of the corresponding tongues (as computed in Ref. [15] with $R_N = 2 \times 10^4$ and $\sigma = 1$). The results, shown in Fig. 5, yield the fits

$$\mathcal{R}(\nabla^2, w_{\boldsymbol{k}}) \approx \delta_{\boldsymbol{k}}\left(1 + \frac{14}{2m^2}\right) \quad \text{and} \quad \mathcal{R}(\nabla^2, \theta_{\boldsymbol{k}}) \approx \delta_{\boldsymbol{k}}\left(1 + \frac{1}{2m^2}\right), \tag{18}$$

which suggest replacing $\delta_{\boldsymbol{k}}$ for general modes $\boldsymbol{k} = m{:}n$ in Eq. (15) with an expression of the form

$$\delta_{\boldsymbol{k}} = -\pi^2(m^2 + n^2)\left(1 + \frac{\gamma}{m^2 + n^2}\right). \tag{19}$$

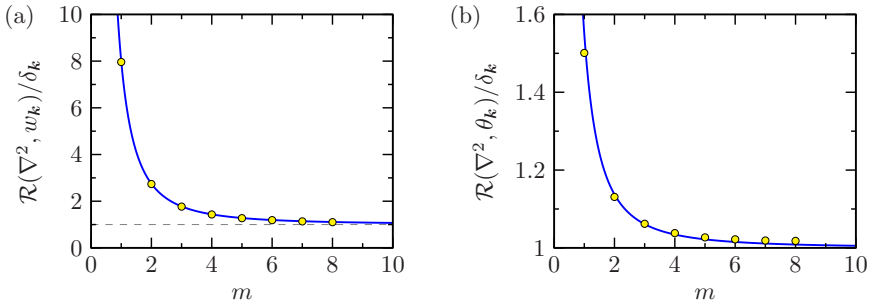

FIG. 5. Scaled diffusion $\nabla^2/\delta_{\boldsymbol{k}}$ applied to viscous Floquet modes (a) $w_{\boldsymbol{k}}$ and (b) $\theta_{\boldsymbol{k}}$ for modes $\boldsymbol{k} = m{:}m$ vs m, as determined by the Rayleigh quotients (17), together with the fits (18).

An additional correction factor to (19),

$$0.75 + \frac{(mn)^2}{(m^2+n^2)^2} = 0.75 + 0.25\sin^2(2\varphi_{\boldsymbol{k}}), \tag{20}$$

where $\tan\varphi_{\boldsymbol{k}} = n/m$ measures the inclination of the wave vector $\boldsymbol{k} = m{:}n$, is also introduced to moderate (by up to 25%) the modal diffusion for vertical and horizontal wave vectors (corresponding to $m \neq n$), associated with forcing frequencies away from $\omega = \sqrt{2}$. The resulting ansatz for $\delta_{\boldsymbol{k}}$,

$$\delta_{\boldsymbol{k}} = -\pi^2(m^2+n^2)\left(1 + \frac{\gamma}{m^2+n^2}\right)\left(0.75 + \frac{(mn)^2}{(m^2+n^2)^2}\right), \tag{21}$$

bears similarities with the expression of the ratio of modal boundary to bulk dissipations from Ref. [7], Eq. (5.5) [e.g., $mn/(m^2+n^2) = \sin^2\varphi_{\boldsymbol{k}}\cot\varphi_{\boldsymbol{k}}$]. However, (21) does not vanish for horizontal wave vectors ($m > n$), whereas boundary dissipation in Ref. [7], Eq. (5.5), does, ignoring contributions from the container's lateral boundaries.

The superposed modal Ince-Strutt stability diagrams, recomputed at $R_{\mathrm{N}} = 2\times10^4$ and $\sigma = 1$ using (21) with $\gamma = 20$, obtained by fitting critical Floquet amplitudes at the $m{:}m$ modes with $1 \leqslant m \leqslant 8$ [and somewhat higher than the values 14 or 1 suggested by (18)], are shown in Fig. 4. They are in excellent agreement with the critical curves obtained via Floquet analysis for both subharmonic and synchronous responses [15]. In particular, our model correctly identifies the rare instances of primary synchronous responses in the lower frequency range. There is a small detuning, particularly for lower ω, which is due to a mild dependence of $\mathcal{L}$ on ω; see Appendix B.

The robustness of the ansatz (21) to changes in both R_{N} and σ was tested by comparing the critical forcing amplitudes obtained at $R_{\mathrm{N}} = 10^4$ and $\sigma = 1$, $R_{\mathrm{N}} = 4\times10^4$ and $\sigma = 1$, and $R_{\mathrm{N}} = 2\times10^4$ and $\sigma = 7$, using the model (21) with an adjusted γ, with those obtained via Floquet analysis. Figure 6 shows the results using $\gamma = 15$, 27, and 30.6, respectively. Again, the match is very good, especially for wave numbers $\boldsymbol{k}$ with low m or n. The subharmonic critical curves obtained for $R_{\mathrm{N}} = 4\times10^4$ and $\sigma = 1$, and $R_{\mathrm{N}} = 2\times10^4$ and $\sigma = 7$, are very similar. The different values of γ are consistent with the scaling

$$\gamma \approx 3 + 0.12\left(\sigma R_{\mathrm{N}}^2\right)^{1/4}, \tag{22}$$

reflecting the balance between momentum diffusion, quantified by R_{N}, and thermal diffusion, quantified by σR_{N}. As R_{N} increases, γ switches from being $O(1)$ to being $O(R_{\mathrm{N}}^{1/2})$. In other words, the dissipation [diagonal coefficients of $A_{\boldsymbol{k}}(t)$ in Eq. (14)] shifts from being $O(R_{\mathrm{N}}^{-1})$, typical of a viscous-dominated regime, to being $O(R_{\mathrm{N}}^{-1/2})$ in the buoyancy-dominated regime. The dependence of γ on R_{N} (22) also yields an estimate of the forcing amplitude at the tip of the principal 1:1 tongue

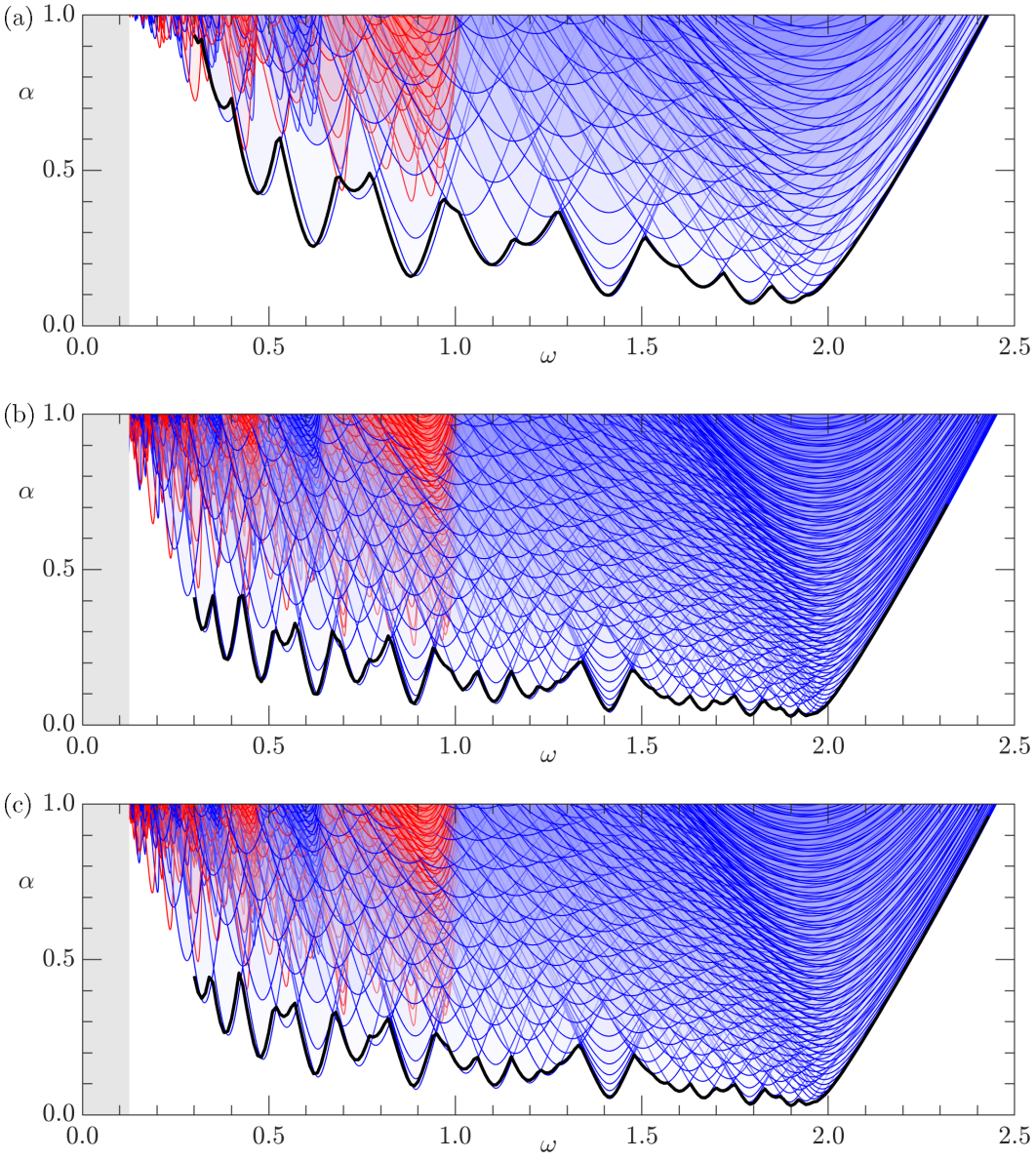

FIG. 6. Same as in Fig. 4 using corrected diagonal coefficients (21) in Eq. (14) with (a) $\gamma = 15$ at $R_N = 10^4$ and $\sigma = 1$, (b) $\gamma = 27$ at $R_N = 4 \times 10^4$ and $\sigma = 1$, and (c) $\gamma = 30.6$ at $R_N = 2 \times 10^4$ and $\sigma = 7$. Only primary subcritical responses at forcing frequencies $\omega \geqslant 0.3$ were computed via Floquet analysis for the sake of efficiency. The MATLAB script `stability_diagram.m` [23] in the Supplemental Material can be used to recreate the modal responses. The movie `movie-fig06.mp4` in the Supplemental Material [23] animates the modal responses for $\sigma = 1$ and $R_N \in [10^3, 10^5]$.

at $\omega \approx \sqrt{2}$:

$$\alpha_{\min} \approx 2Q_{1:1} = \frac{4\delta_{1:1}}{R_N\sqrt{\lambda_{1:1}}} \approx \frac{279}{R_N} + \frac{6.7}{\sqrt{R_N}} \tag{23}$$

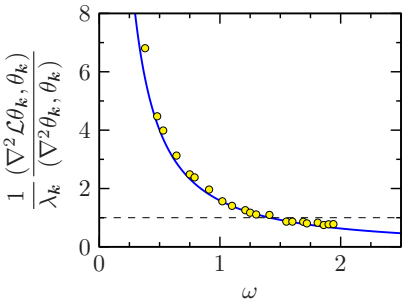

FIG. 7. Scaled operator $\mathcal{L}/\lambda_k$ applied to viscous Floquet mode θ_k vs forcing frequency ω, together with the fit $(\omega/\sqrt{2})^{-4/3}$.

at $\sigma = 1$, in good general agreement with the results presented in Ref. [15], Fig. 7(b). The balance between the two terms on the right-hand side of (23) occurs at a relatively low $R_{\mathrm{N}} \approx 1734$, while the last term accounts for 78% at $R_{\mathrm{N}} = 2 \times 10^4$.

IV. CONCLUSIONS

Confinement together with viscous effects make the determination of neutral curves in large parametric studies of fluid flows subjected to parametric forcing a nontrivial task due to the noncommutation of operators ($\mathcal{L}$ and ∇^2). We have shown how global neutral curves can still be obtained via superposition of modal responses, provided a suitable model of viscous dissipation based on interpolation of local Floquet data at the onset of instability is used to account for boundary layer contributions. The specific dissipation model used is problem-dependent and must be adjusted accordingly. In our study, we have considered parameter regimes where dissipation is dominated by viscous boundary layer effects, corresponding to $R_N \gtrsim 10^3$. We have demonstrated that it correctly predicts the onset of instability for $10^3 \leqslant R_N \leqslant 10^5$. For $R_N \lesssim 400$, the linearly stratified base state remains stable for all forcing amplitudes $\alpha < 1$ and forcing frequencies ω, so there is no parametric instability to test the model against. Nevertheless, the model correctly predicts the base state to be stable for $\alpha < 1$ and $R_N \lesssim 400$.

It is expected that the interpolatory approach presented here, consisting of using selected Floquet data to calibrate the dissipation model used and bypass restrictions due to the noncommutation of operators, can be generalized to other systems, including three-dimensional configurations or more general Hill-type periodic parametric forcings, at least as long as the primary bifurcation of the base state in modal responses occurs in a similar way as it does in the full system (excluding, for example, the possibility of "combination resonances" [22] in Mathieu PDEs, which do not occur in the scalar version).

ACKNOWLEDGMENTS

We thank Research Computing at Arizona State University and the NSF XSEDE program for providing the High Performance Computing and storage resources necessary to conduct the Floquet analysis.

APPENDIX A

Equation (16) is written

$$\theta_k'' + c_k\theta_k' + (a_k + 2q_k\cos\omega t)\theta_k = 0, \tag{A1}$$

with

$$c_k = -\frac{1}{R_{\mathrm{N}}}\left(1 + \frac{1}{\sigma}\right)\delta_k, \quad a_k = \frac{1}{\sigma R_{\mathrm{N}}^2}\delta_k^2 + \lambda_k, \quad 2q_k = \alpha\lambda_k. \tag{A2}$$

According to Floquet theory, the trivial state $\theta_{\boldsymbol{k}} = 0$ loses stability to a solution of the form

$$\theta_{\boldsymbol{k}} = e^{i\mu t} \sum_{n\in\mathbb{Z}} \widehat{\theta}_{\boldsymbol{k},n} e^{in\omega t}, \tag{A3}$$

with either $\mu = 0$ (synchronous solutions) or $\mu = \omega/2$ (subharmonic solutions) [4].

Substituting (A3) into (A1) yields an infinite Hill system of linear equations for the coefficients $\widehat{\theta}_{\boldsymbol{k},n}$, whose determinant

$$\Delta_{\boldsymbol{k}} = \det[\mathrm{tridiag}(q_{\boldsymbol{k}}, d_{\boldsymbol{k},n}, q_{\boldsymbol{k}})]_{n\in\mathbb{Z}}, \tag{A4}$$

where

$$d_{\boldsymbol{k},n} = a_{\boldsymbol{k}} - (n\omega + \mu)^2 + ic_{\boldsymbol{k}}(n\omega + \mu), \tag{A5}$$

vanishes. Substituting (A2) into the equation $\Delta_{\boldsymbol{k}} = 0$ reduces it to a generalized eigenvalue problem (for each μ) for the critical α at fixed ω, as was done in Ref. [4] for the Faraday problem. Instead, (a truncated version of) $\Delta_{\boldsymbol{k}}$ is evaluated on a (fine) grid in (ω, α) parameter space via an LU factorization (for each grid point), with its 0 locus obtained via interpolation. The truncation of $\Delta_{\boldsymbol{k}}$ to a range $-N \leqslant n \leqslant M$, with $M = N - 1$ if $\mu = 0$ and $M = N$ if $\mu = \omega/2$, yields a determinant $\Delta_{\boldsymbol{k},N}$ that is guaranteed to be real due to its centro-Hermitian property [24] ($N = 60$ was used). Partitioning $\Delta_{\boldsymbol{k},N}$ as

$$\Delta_{\boldsymbol{k},N} = \det \begin{bmatrix} A_{\boldsymbol{k},N} & q_{\boldsymbol{k}} \boldsymbol{e}_N \boldsymbol{e}_1^T \\ q_{\boldsymbol{k}} \boldsymbol{e}_1 \boldsymbol{e}_N^T & B_{\boldsymbol{k},N} \end{bmatrix}, \tag{A6}$$

with

$$A_{\boldsymbol{k},N} = \begin{bmatrix} d_{\boldsymbol{k},-N} & q_{\boldsymbol{k}} & & \\ \ddots & \ddots & \ddots & \\ & q_{\boldsymbol{k}} & d_{\boldsymbol{k},-1} \end{bmatrix}, \quad \boldsymbol{e}_1 = \begin{bmatrix} 1 \\ \vdots \\ 0 \end{bmatrix}, \quad \boldsymbol{e}_N = \begin{bmatrix} 0 \\ \vdots \\ 1 \end{bmatrix}, \quad B = \begin{bmatrix} d_{\boldsymbol{k},0} & q_{\boldsymbol{k}} & & \\ \ddots & \ddots & \ddots & \\ & q_{\boldsymbol{k}} & d_{\boldsymbol{k},M} \end{bmatrix}, \tag{A7}$$

yields (assuming $A_{\boldsymbol{k},N}$ and $B_{\boldsymbol{k},N}$ are nonsingular)

$$\begin{aligned} \Delta_{\boldsymbol{k},N} &= \det(A_{\boldsymbol{k},N}) \det\left(B_{\boldsymbol{k},N} - q_{\boldsymbol{k}}^2 \boldsymbol{e}_1 \boldsymbol{e}_N^T A_{\boldsymbol{k},N}^{-1} \boldsymbol{e}_N \boldsymbol{e}_1^T\right) \\ &= \det(A_{\boldsymbol{k},N}) \det(B_{\boldsymbol{k},N}) \det\left(I - q_{\boldsymbol{k}}^2 B_{\boldsymbol{k},N}^{-1} \boldsymbol{e}_1 \boldsymbol{e}_N^T A_{\boldsymbol{k},N}^{-1} \boldsymbol{e}_N \boldsymbol{e}_1^T\right) \\ &= \det(A_{\boldsymbol{k},N}) \det(B_{\boldsymbol{k},N}) \left(1 - q_{\boldsymbol{k}}^2 \left(\boldsymbol{e}_1^T B_{\boldsymbol{k},N}^{-1} \boldsymbol{e}_1\right) \left(\boldsymbol{e}_N^T A_{\boldsymbol{k},N}^{-1} \boldsymbol{e}_N\right)\right). \end{aligned}$$

The quantity $\boldsymbol{e}_N^T A_{\boldsymbol{k},N}^{-1} \boldsymbol{e}_N$ is the trailing (bottom right) coefficient of $A_{\boldsymbol{k},N}^{-1}$, equal to the inverse, $1/(U_{\boldsymbol{k},N})_{N,N}$, of the trailing diagonal coefficient $(U_{\boldsymbol{k},N})_{N,N}$ of the upper triangular matrix $U_{\boldsymbol{k},N}$ in the LU factorization of $A_{\boldsymbol{k},N}$. This coefficient can be determined via a recurrence

$$\begin{aligned} &(U_{\boldsymbol{k},N})_{0,0} = \infty, \\ &(U_{\boldsymbol{k},N})_{n,n} = d_{\boldsymbol{k},n-1-N} - q_{\boldsymbol{k}}^2/(U_{\boldsymbol{k},N})_{n-1,n-1}, \quad n = 1, \ldots, N, \end{aligned} \tag{A8}$$

expressing it as a continued fraction of $q_{\boldsymbol{k}}^2$. As a result:

(i) If $\mu = \omega/2$, the centro-Hermitian property of $\Delta_{\boldsymbol{k},N}$ implies $\boldsymbol{e}_1^T B_{\boldsymbol{k},N}^{-1} \boldsymbol{e}_1 = \overline{\boldsymbol{e}_N^T A_{\boldsymbol{k},N}^{-1} \boldsymbol{e}_N}$, so that $\Delta_{\boldsymbol{k},N} = 0$ reduces to

$$|(U_{\boldsymbol{k},N})_{N,N}| = q_{\boldsymbol{k}}. \tag{A9}$$

(ii) By analogy, for $\mu = 0$, $\boldsymbol{e}_1^T B_{\boldsymbol{k},N}^{-1} \boldsymbol{e}_1$ is the conjugate of the trailing coefficient in the inverse of the $(N + 1) \times (N + 1)$ matrix

$$\begin{bmatrix} A_{\boldsymbol{k},N} & q_{\boldsymbol{k}} \boldsymbol{e}_N \\ q_{\boldsymbol{k}} \boldsymbol{e}_N^T & d_{\boldsymbol{k},0} \end{bmatrix},$$

which is equal to the conjugate of the inverse of the coefficient $(U_{\boldsymbol{k},N})_{N+1,N+1}$, obtained by extending (A8) to $n = N + 1$. In this case, $\Delta_{\boldsymbol{k},N} = 0$ reduces to $(U_{\boldsymbol{k},N})_{N,N}\overline{(U_{\boldsymbol{k},N})_{N+1,N+1}} = q_{\boldsymbol{k}}^2$, i.e.,

$$\sqrt{|(U_{\boldsymbol{k},N})_{N,N}(U_{\boldsymbol{k},N})_{N+1,N+1}|} = q_{\boldsymbol{k}}. \tag{A10}$$

The relations (A9) and (A10), respectively, determine the subcritical and synchronous stability tongues of (A1), and they are implemented in the Supplemental Material MATLAB program `stability_diagram.m` [23].

APPENDIX B

The action of $\mathcal{L}$ on the viscous modes $\theta_{\boldsymbol{k}}$ cannot be directly quantified using a standard L_2-norm based Rayleigh quotient, $\mathcal{R}(\mathcal{L}, \theta_{\boldsymbol{k}})$, because an explicit expression for the action of $\mathcal{L}$ on $\theta_{\boldsymbol{k}}$ is not directly available. Instead, we use a Rayleigh quotient based on a norm associated with $-\nabla^2$:

$$\frac{(\mathcal{L}\theta_{\boldsymbol{k}}, \theta_{\boldsymbol{k}})_{-\nabla^2}}{(\theta_{\boldsymbol{k}}, \theta_{\boldsymbol{k}})_{-\nabla^2}} = \frac{(-\nabla^2\mathcal{L}\theta_{\boldsymbol{k}}, \theta_{\boldsymbol{k}})}{(-\nabla^2\theta_{\boldsymbol{k}}, \theta_{\boldsymbol{k}})} = \frac{\left(-\partial_x^2\theta_{\boldsymbol{k}}, \theta_{\boldsymbol{k}}\right)}{\|\nabla\theta_{\boldsymbol{k}}\|^2} = \frac{\|\partial_x\theta_{\boldsymbol{k}}\|^2}{\|\nabla\theta_{\boldsymbol{k}}\|^2}. \tag{B1}$$

In the inviscid limit, this quotient reduces to $\lambda_{\boldsymbol{k}} = m^2/(m^2 + n^2)$ for Floquet mode $\boldsymbol{k} = m{:}n$. Viscous effects were evaluated on the modes obtained from Floquet analysis at various forcing frequencies ω for the case $R_{\mathrm{N}} = 2 \times 10^4$ and $\sigma = 1$. Figure 7 shows the deviation of the Rayleigh quotients (B1), scaled by $\lambda_{\boldsymbol{k}}$, from unity (dashed line), together with a fit $(\omega/\sqrt{2})^{-4/3}$. In particular, $\lambda_{\boldsymbol{k}}$ underestimates (overestimates) $\mathcal{L}$ for $\omega < \sqrt{2}$ ($\omega > \sqrt{2}$) corresponding to modes $\boldsymbol{k}$ with $m < n$ ($m > n$). This discrepancy causes a small detuning of the modal tongues toward the frequency $\omega = \sqrt{2}$, which is clearly visible at lower ω in Figs. 4 and 6.

The symmetry of $\mathcal{L}$ with respect to $-\nabla^2$ follows from

$$(\mathcal{L}\theta_{\boldsymbol{k}}, \theta_{\boldsymbol{\ell}})_{-\nabla^2} = (\partial_x\theta_{\boldsymbol{k}}, \partial_x\theta_{\boldsymbol{\ell}}) = (\mathcal{L}\theta_{\boldsymbol{\ell}}, \theta_{\boldsymbol{k}})_{-\nabla^2}, \tag{B2}$$

and (B1) shows that

$$\|\mathcal{L}\|_{-\nabla^2} = \sup\{|(\mathcal{L}\theta, \theta)_{-\nabla^2}|, \|\theta\|_{-\nabla^2} = 1\} \leqslant 1. \tag{B3}$$

In the confined case, $\mathcal{L}$ does not commute with ∇^2. This is the reason why (8) cannot be simply reduced to simple modal responses. Instead, $\nabla^2\mathcal{L} = \widehat{\mathcal{L}}\nabla^2$, for a different symmetric linear operator $\widehat{\mathcal{L}}$. In the two-dimensional setting, $\widehat{\mathcal{L}} = \partial_x\nabla_0^{-2}\partial_x$ provides an explicit expression for $\widehat{\mathcal{L}}$, where $\nabla_0^{-2}\varphi$ denotes the solution of a Poisson problem, $\nabla^2\psi = \varphi$, with homogeneous boundary conditions. Indeed, the boundary condition $\partial_x\theta = 0$ on all walls yields

$$\widehat{\mathcal{L}}\nabla^2\theta = \partial_x\nabla_0^{-2}\partial_x\nabla^2\theta = \partial_x\nabla_0^{-2}\nabla^2\partial_x\theta = \partial_x^2\theta = \nabla^2\mathcal{L}\theta. \tag{B4}$$

The system (8) can then be expressed in terms of $\widehat{\mathcal{L}}$ as

$$\partial_t\begin{bmatrix}\nabla^2 w\\ \nabla^2\theta\end{bmatrix} = \widehat{\mathcal{A}}(t)\begin{bmatrix}\nabla^2 w\\ \nabla^2\theta\end{bmatrix}, \quad \widehat{\mathcal{A}}(t) = \begin{bmatrix}\frac{1}{R_{\mathrm{N}}}\nabla^2 & f(t)\widehat{\mathcal{L}}\\ -\mathcal{I} & \frac{1}{\sigma R_{\mathrm{N}}}\nabla^2\end{bmatrix}. \tag{B5}$$

However, (B5) requires more regularity on w and θ compared to (8) (the state variables are now $\nabla^2 w$ and $\nabla^2\theta$), hindering the numerical estimation of modal actions via Rayleigh quotients, as in Figs. 5 and 7.

[1] T. B. Benjamin and F. Ursell, The stability of the plane free surface of a liquid in vertical periodic motion, Proc. R. Soc. London A **225**, 505 (1954).

[2] C.-S. Yih, Gravity waves in a stratified fluid, J. Fluid Mech. **8**, 481 (1960).

[3] S. A. Thorpe, On standing internal gravity waves of finite amplitude, J. Fluid Mech. **32**, 489 (1968).
[4] K. Kumar and L. S. Tuckerman, Parametric instability of the interface between two fluids, J. Fluid Mech. **279**, 49 (1994).
[5] J. Wright, S. Yon, and C. Pozrikidis, Numerical studies of two-dimensional Faraday oscillations of inviscid fluids, J. Fluid Mech. **402**, 1 (2000).
[6] F. J. Mancebo and J. M. Vega, Faraday instability threshold in large-aspect-ratio containers, J. Fluid Mech. **467**, 307 (2002).
[7] D. Benielli and J. Sommeria, Excitation and breaking of internal gravity waves by parametric instability, J. Fluid Mech. **374**, 117 (1998).
[8] R. M. Carbo, R. W. M. Smith, and M. E. Poese, A computational model for the dynamic stabilization of Rayleigh-Bénard convection in a cubic cavity, J. Acoust. Soc. Am. **135**, 654 (2014).
[9] E. Knobloch, C. Martel, and J. M. Vega, Coupled mean flow-amplitude equations for nearly inviscid parametrically driven surface waves, Ann. N.Y. Acad. Sci. **974**, 201 (2002).
[10] K. Kumar, Linear theory of Faraday instability in viscous liquids, Proc. R. Soc. London A **452**, 1113 (1996).
[11] H. W. Müller, H. Wittmer, C. Wagner, J. Albers, and K. Knorr, Analytic Stability Theory for Faraday Waves and the Observation of the Harmonic Surface Response, Phys. Rev. Lett. **78**, 2357 (1997).
[12] J. Rajchenbach and D. Clamond, Faraday waves: Their dispersion relation, nature of bifurcation and wavenumber selection revisited, J. Fluid Mech. **777**, R2 (2015).
[13] E. Cerda and E. Tirapegui, Faraday's Instability for Viscous Fluids, Phys. Rev. Lett. **78**, 859 (1997).
[14] R. A. Ibrahim, Recent advances in physics of fluid parametric sloshing and related problems, ASME J. Fluid Eng. **137**, 090801 (2015).
[15] J. Yalim, J. M. Lopez, and B. D. Welfert, Vertically forced stably stratified cavity flow: Instabilities of the basic state, J. Fluid Mech. **851**, R6 (2018).
[16] J. Yalim, B. D. Welfert, and J. M. Lopez, Parametrically forced stably stratified cavity flow: Complicated nonlinear dynamics near the onset of instability, J. Fluid Mech. **871**, 1067 (2019).
[17] E. Mathieu, Mémoire sur le mouvement vibratoire d'une membrane de forme elliptique, J. Math. Pures Appl. **13**, 137 (1868).
[18] L. Ruby, Applications of the Mathieu equation, Am. J. Phys. **64**, 39 (1996).
[19] K. L. Turner, S. A. Miller, P. G. Hartwell, N. C. MacDonald, S. H. Strogatz, and S. G. Adams, Five parametric resonances in a microelectromechanical system, Nature (London) **396**, 149 (1998).
[20] N. W. McLachlan, *Theory and Applications of Mathieu Functions* (Oxford University Press, Oxford, 1947).
[21] I. Kovacic, R. Rand, and S. M. Sah, Mathieu's equation and its generalizations: Overview of stability charts and their features, Appl. Mech. Rev. **70**, 020802 (2018).
[22] A. Champneys, Dynamics of parametric excitation, in *Mathematics of Complexity and Dynamical Systems*, edited by R. A. Meyers (Springer, New York, 2012), pp. 183–204.
[23] See Supplemental Material at http://link.aps.org/supplemental/10.1103/PhysRevFluids.4.103903 for a Matlab script and an animation corresponding to Fig. 6.
[24] A. Lee, Centrohermitian and skew-centrohermitian matrices, Lin. Alg. Appl. **29**, 205 (1980).